

Low-energy excitations around $(\frac{\pi}{2}, \frac{\pi}{2})$ points in the pseudogap phase of $\text{Nd}_{1.85}\text{Ce}_{0.15}\text{CuO}_4$

A. Koitzsch^{1,†}, G. Blumberg^{1,§}, A. Gozar¹, B.S. Dennis¹, P. Fournier^{2,¶}, and R.L. Greene²

¹*Bell Laboratories, Lucent Technologies, Murray Hill, New Jersey 07974*

²*Center for Superconductivity Research and Department of Physics, University of Maryland, College Park, MD 20742*
(November 1, 2018)

Polarized electronic Raman scattering from the $\text{Nd}_{1.85}\text{Ce}_{0.15}\text{CuO}_4$ superconductor at optimal electron doping ($T_c = 22$ K) reveals the formation of an anisotropic pseudogap below a characteristic temperature $T^* \approx 220$ K and energy $E_g^* = 850 \text{ cm}^{-1}$. Below T^* a pronounced suppression of the incoherent spectral weight below E_g^* in the nodal directions of \mathbf{k} -space is observed. This is concomitant with the emergence of long-lived excitations in the vicinity of the $(\pm\pi/2, \pm\pi/2)$ points that do not contribute to the optical conductivity.

PACS numbers: 74.25.Gz, 74.72.Jt, 78.30.-j

The origin of the pseudogap (PG) in cuprate superconductors is believed to lie at the heart of a general understanding of superconductivity in this material class. A large body of experimental results have been collected for hole doped cuprates and many theoretical approaches have been developed [1]. A consensus on the underlying mechanism is still far from being reached. Recently studies of electron doped cuprates have shifted under focus, first, with the reexamination of the symmetry of the order parameter [2–8] whereby a $d_{x^2-y^2}$ symmetry was established for under- and optimal doping, and second, with the investigation of the PG [9–13]. It was also found that electron doped cuprates violate the Wiedemann-Franz law, indicating the breakdown of Fermi liquid theory [14]. These materials offer the unique possibility of comparison with their hole doped counterparts which can serve as a touchstone for theory. Furthermore, electron doped materials like $\text{Nd}_{1.85}\text{Ce}_{0.15}\text{CuO}_4$ (NCCO) show their own peculiarities. The doping range where the superconducting (SC) transition occurs is much narrower than for hole doped cuprates and the maximum achievable SC transition temperatures (T_c) are much lower. Also, the normal state in-plane-resistivity shows a tendency to a quadratic temperature dependence [15] in contrast to the optimally hole doped cuprates where the dependence is linear [16].

While PG phenomena for hole doped cuprates was investigated by a large number of experimental probes the evidence for a PG in electron doped cuprates is still limited. A recent optics study has found a large PG for underdoped NCCO [12]. For optimally doped NCCO it has been shown that the scattering rate extracted from optical conductivity, $\sigma(\omega)$, is suppressed below certain energies and temperatures [9,10]. The ARPES experiment showed regions of suppressed intensity at the Fermi surface (FS) with a broad peak at about 100 meV ($\approx 800 \text{ cm}^{-1}$) at low temperatures [11]. These regions are shifted closer to the nodal directions with respect to the hole doped cuprates. On the other hand, c -axis tunneling studies did not indicate PG suppression above T_c

[17,18].

Here we report a Raman study of NCCO in the PG phase. In contrast to the observations for hole doped cuprates, for NCCO, a substantial suppression of the Raman response below an onset temperature $T^* \approx 220$ K and a threshold energy $E_g^* = 850 \text{ cm}^{-1}$ was observed for the symmetry that probes excitations in the proximity of the nodal directions of \mathbf{k} -space. Furthermore, we found novel long lived low energy excitations that reside in the vicinity of $(\pm\pi/2, \pm\pi/2)$ regions in the PG phase but do not show an observable contribution to the optical conductivity. The excitations in the proximity of the Brillouin zone (BZ) boundaries observed by Raman scale to the optical conductivity data.

The Raman experiments were performed from a natural ab surface of plate-like single crystals grown as described in Ref. [19]. After growth, the crystals were annealed in an oxygen-reduced atmosphere to induce the doping level for an optimal T_c . The SC transition measured by SQUID was about 22 K with a width of about 2 K. The sample was mounted in an optical continuous helium flow cryostat. Spectra were measured in a backscattering geometry using the 6471 Å excitation of a Kr^+ laser. An incident laser power less than 10 mW was focused to a 50 μm spot on the sample surface. The referred temperatures were corrected for estimated laser heating. The spectra were analyzed by a custom triple grating spectrometer and were corrected for the instrumental response.

The presented data were taken in (xy) and $(x'y')$ scattering geometries, with $x = [100]$, $y = [010]$, $x' = [110]$, and $y' = [\bar{1}10]$. For tetragonal D_{4h} symmetry the (xy) and $(x'y')$ geometries correspond to spectra of $\text{B}_{2g} + \text{A}_{2g}$ and $\text{B}_{1g} + \text{A}_{2g}$ representations. Measurements in an external magnetic field have been performed with circularly polarized light where a right-left (RL) scattering geometry corresponds to spectra of $\text{B}_{1g} + \text{B}_{2g}$ representation. In addition, by using right-right (RR) geometry, we checked the intensity of the A_{2g} component and found

it to be negligibly weak.

The electronic Raman response function for a given scattering geometry is proportional to the sum over the density of states at the FS weighted by a momentum \mathbf{k} dependent Raman form factor. By choosing the scattering geometry one can selectively probe different regions of the FS. In the insets of Fig. 1 we sketch the first BZ for NCCO as suggested by ARPES data [4,5,11]. The shaded area corresponds to occupied electron states. For the B_{2g} channel the Raman form factor vanishes along $(0,0) \rightarrow (\pi,0)$ and the equivalent lines of \mathbf{k} -space. The Raman response projects out excitations in the vicinity of $(\pm\pi/2, \pm\pi/2)$ points of the BZ. In contrast, the B_{1g} intensity vanishes along the diagonals and the intensity is collected from the regions of the BZ distant from the diagonals. The 45° rotated square indicates the antiferromagnetic Brillouin zone (AF BZ). Intersections of the FS and the AF BZ are marked in the upper left quadrant with black circles. These points are connected by the AF unit vector (π, π) .

In Fig. 1 we show the Raman response as a function of temperature for the B_{1g} and B_{2g} channels. For B_{2g} symmetry two distinct features develop in the spectra with cooling:

(i) A "knee" like intensity loss of the Raman response below 850 cm^{-1} . This suppression of spectral weight starts at $T_{B_{2g}}^* \approx 220 \text{ K}$. It deepens with cooling and decreasing energy yielding an almost linear slope of the spectra between 300 and 850 cm^{-1} . We identify this suppression as the opening of a PG with a temperature independent energy scale.

(ii) An overdamped peak is seen at about 350 cm^{-1} at room temperature. This peak sharpens with cooling and shifts to lower frequencies from 150 cm^{-1} at 220 K to 25 cm^{-1} at 35 K . We refer to this feature as a quasi-elastic scattering peak (QEP).

The opening of the PG with a similar energy scale is also present but not as pronounced in the B_{1g} channel. The QEP however is much weaker and at higher energies.

In contrast, for hole doped cuprates the PG suppression is most pronounced for the B_{1g} channel [21–26]. For hole underdoped cuprates a destruction of the FS near its intersection with AF BZ boundary has been observed [27,28]. Therefore Raman scattering for the B_{1g} symmetry is suppressed leaving only small PG effects for the B_{2g} channel [22,29,30].

A conjecture that the PG opens up at the intersections of the AF BZ and FS, the *hot spots* [31–34], reconciles the observed differences for the electron and hole doped materials. Strong antiferromagnetic interactions suppress the spectral weight at the chemical potential in the *hot spots* leading to a "destruction" of the FS in this region of \mathbf{k} -space and opening of the PG. In hole doped cuprates *hot spots* are located closer to the $(\pi, 0)$ points while for electron doping the FS shrinks shifting *hot spots* closer to the nodal directions [6,11,27]. Hence, for the hole under-

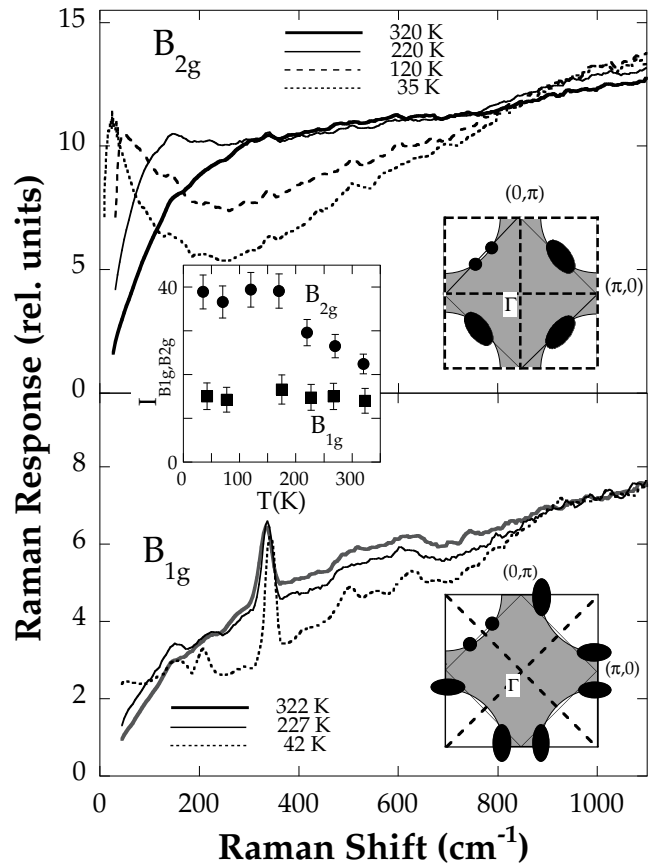


FIG. 1. Raman response function for B_{2g} and B_{1g} symmetry channels (1.9 eV excitation) at temperatures between 35 and 320 K. Sketches for the Fermi surface are based on ARPES data [4,5,11]. Regions where the Raman form-factor is maximal are denoted by black ellipses; the nodal regions are shown by dashed lines. The antiferromagnetic Brillouin zone is indicated as a square rotated by 45° . AF fluctuations enhance interactions between fermions around the *hot spots* (filled circles). The sharp modes for B_{1g} are phonons [20]. The inset shows $I_\mu = \int_0^{850} \chi''_\mu / \omega d\omega$ for $\mu = B_{1g}$ (squares) and B_{2g} (circles).

doped systems the PG is more pronounced in B_{1g} while for electron doped systems in the B_{2g} scattering channel.

Cooling the sample below $T_c = 22 \text{ K}$ leads to opening of the SC gap and formation of a pair breaking 2Δ peak [6]. The QEP is suppressed in this regime. An applied magnetic field up to 9 T did not influence either the PG or the QEP above T_c . In contrast, below T_c an external magnetic field of this magnitude strongly suppresses SC correlations [35] and reveals the underlying QEP (See Fig. 2).

In Fig. 2 we show the low frequency part of the Raman response in the B_{2g} channel. The QEP develops with decreasing temperature. It is also present at temperatures below T_c if superconductivity is suppressed by a magnetic field [36]. We fit the low energy B_{2g} response

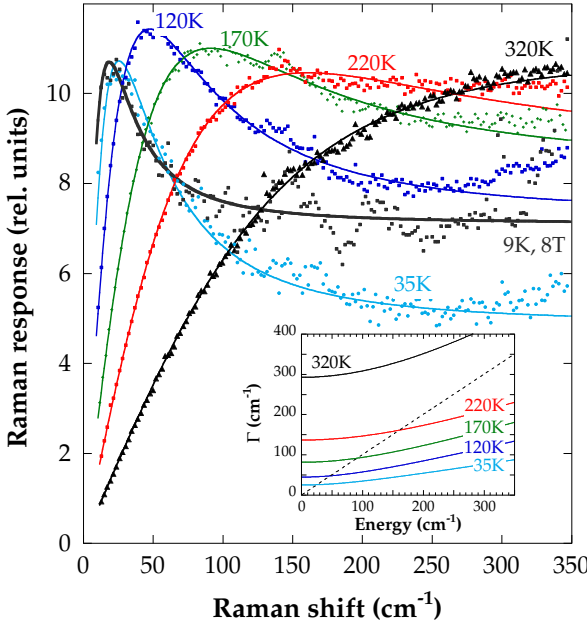


FIG. 2. Low frequency Raman response for the B_{2g} channel between 35 and 320 K. The quasi-elastic peak develops with cooling. The 9 K spectra was measured in an external magnetic field applied parallel to the c -axis in RL-polarization ($B_{1g} + B_{2g}$ channel). The solid lines are fits to the extended Drude model (1). Inset: Frequency dependent scattering rate $\Gamma^{B_{2g}}(\omega, T)$ resulting from the fits to the Drude model (1) for temperatures between 35 and 320 K. The dashed $\Gamma = \omega$ line represents a crossover from an overdamped regime to longer lived excitations.

by an extended Drude model:

$$\chi''(\omega, T) \propto N_F^{B_{2g}} \frac{\omega \Gamma^{B_{2g}}(\omega, T)}{\omega^2 + \Gamma^{B_{2g}}(\omega, T)^2}, \quad (1)$$

where $N_F^{B_{2g}}$ is the density of states at the Fermi level weighted by a symmetry dependent Raman form factor and $\Gamma^{B_{2g}}(\omega, T)$ is a frequency and energy dependent scattering rate. The scattering rate $\Gamma^{B_{2g}}(\omega, T)$ for different temperatures extracted from the extended Drude fits is shown in the inset of Fig. 2. $\Gamma^{B_{2g}}$ is about 300 cm^{-1} at room temperature and decreases rapidly with cooling. The small variation with frequency suggests that a simple Drude model is a good description of the data. However, qualitative differences appear when the momentum dependence of the scattering rate is analyzed.

In Fig. 3 we compare optical conductivity and χ''/ω for $\mu = B_{2g}$ and B_{1g} channels between 35 and 300 K. In the lowest order approximation $\chi''_\mu(\omega)/\omega$ is proportional to optical conductivity weighted by a geometrical Raman form factor [37]. We notice that the Drude response narrows with cooling for $\sigma(\omega)$ as well as for χ''/ω in both $\mu = B_{2g}$ and B_{1g} channels. For B_{1g} the width of the peak decreases from above 400 cm^{-1}

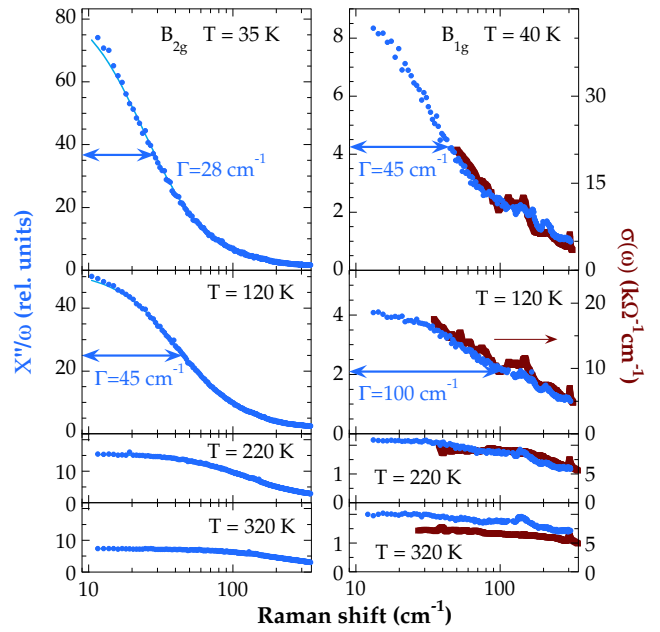


FIG. 3. χ''_μ/ω response for $\mu = B_{2g}$ and B_{1g} channels (dots in left and right panels) between 35 K and 320 K. The optical conductivity (thick dark solid line) is shown on the right scale [9] and is consistent with $\chi''_{B_{1g}}/\omega$. The thin solid lines on the left represent the fit to the extended Drude model (1). Phonons have been removed from the B_{1g} spectra.

around room temperature to 45 cm^{-1} above the superconducting transition, retaining however a value about twice that of the B_{2g} channel at corresponding temperatures. This difference implies a momentum dependence of the scattering rate: a longer lifetime for excitations in the vicinity of $(\pm\pi/2, \pm\pi/2)$ points and more incoherence for excitations around the BZ boundaries. Our observation of increased coherence in the B_{2g} channel is consistent with ARPES results, where the quasi-particle peak linewidth at the Fermi energy decreases in going from the BZ boundary to $(\pi/2, \pi/2)$ point [11].

The momentum dependence of the scattering rate is consistent with the high frequency Raman data (Fig. 1). In the inset of Fig. 1 we present $I_\mu = \int_0^{850} \chi''_\mu/\omega d\omega$ ($\mu = B_{1g}, B_{2g}$) as a function of temperature [38]. While $I_{B_{1g}}$ is a constant $I_{B_{2g}}$ increases with cooling until 170 K indicating a shift of spectral weight from regions beyond 850 cm^{-1} to the lower frequencies [38]. The pronounced suppression of the B_{2g} Raman continuum intensity is another indication of increased coherence at low energies for excitations in the vicinity of $(\pm\pi/2, \pm\pi/2)$ points.

On the right side of Fig. 3 we also plot optical conductivity from Ref. [9]. Surprisingly, $\sigma(\omega)$ exhibits almost perfect scaling to $\chi''_{B_{1g}}(\omega)/\omega$ Raman data: the scaling factor for the double vertical axes was determined for $T = 120 \text{ K}$ data and then used for all temperatures. The

fact that the B_{1g} response bears out the pseudoidentity $\text{Re } \sigma \propto \chi''_{B_{1g}}(\omega)/\omega$ [37] suggests that quasi-particle contributions to the low frequency and *dc* conductivities are dominated by parts of the Fermi surface away from the $(0,0) \rightarrow (\pi,\pi)$ diagonal. The more coherent excitations in the vicinity of $(\pm\pi/2, \pm\pi/2)$ points do not contribute significantly to the optical response. Nevertheless the latter excitations dominate the low frequency B_{2g} Raman response in the PG state. Although further studies are necessary, we suggest that these chargeless excitations may be responsible for the excessive heat transport that leads to the Wiedemann-Franz law violation [14].

In summary, we study charge carrier relaxation dynamics in the PG phase of NCCO. We observe suppression of spectral weight below 850 cm^{-1} for the B_{2g} Raman response and identify it as an anisotropic PG in the vicinity of $(\pm\pi/2, \pm\pi/2)$ points of the BZ. We propose that the PG originates from enhanced AF interactions in *hot spot* regions, which for electron doped cuprates, in contrast to hole doped, are located closer to $(\pm\pi/2, \pm\pi/2)$ points than to the BZ boundary. For the Raman response in the B_{2g} channel we observe a narrow Drude-like QEP in the PG phase. This QEP reveals the emergence of novel long lived excitations in the vicinity of the $(\pm\pi/2, \pm\pi/2)$ points that do not contribute to optical conductivity. In contrast, the excitations in the B_{1g} Raman response were found to be in agreement with optical conductivity data.

AK acknowledges partial support by the Studienstiftung des Deutschen Volkes. RLG acknowledges support by NSF grant DMR-0102350. PF acknowledges the support from CIAR, NSERC and the Foundation FORCE (Sherbrooke). We thank C. Homes for providing the optical conductivity data. AK acknowledges discussions with S.V. Borisenko and T. Pichler.

- [10] E.J. Singley *et al.*, Phys. Rev. B **64**, 224503 (2001).
- [11] N.P. Armitage *et al.*, Phys. Rev. Lett. **87**, 147003 (2001).
- [12] Y. Onose *et al.*, Phys. Rev. Lett. **82**, 5120 (1999); Phys. Rev. Lett. **87**, 217001 (2001).
- [13] T. Tohyama and S. Maekawa, cond-mat/0106311 (2001).
- [14] R.W. Hill *et al.*, Nature **414**, 711 (2001).
- [15] C.C. Tsuei *et al.*, Physica C **161**, 415 (1989).
- [16] M. Gurvich *et al.*, Phys. Rev. Lett. **59**, 1337 (1987).
- [17] S. Kleefisch *et al.*, Phys. Rev. B. **63**, 100507 (2001).
- [18] A. Biswas *et al.*, Phys. Rev. B. **64**, 104519 (2001).
- [19] J.L. Peng *et al.*, Physica C **177**, 79 (1991).
- [20] E.T. Heyen *et al.*, Phys. Rev. B **43**, 2857 (1991).
- [21] F. Slakey *et al.*, Phys. Rev. B **42**, 2643 (1990).
- [22] G. Blumberg *et al.*, Science **278**, 1427 (1997).
- [23] X.K. Chen *et al.*, Phys. Rev. B **56**, R513 (1997).
- [24] J.W. Quilty *et al.*, Phys. Rev. B **57**, R11097 (1998).
- [25] J.G. Naeini *et al.*, Phys. Rev. B **59**, 9642 (1999).
- [26] J. Bäckström *et al.*, Phys. Rev. B **61**, 7049 (2000).
- [27] D.S. Marshall *et al.*, Phys. Rev. Lett. **76**, 4841 (1996).
- [28] M.R. Norman *et al.*, Nature (London) **392**, 157 (1998).
- [29] R. Nemetschek *et al.*, Phys. Rev. Lett. **78**, 4837 (1997).
- [30] M. Opel *et al.*, Phys. Rev. B **61**, 9752 (2000).
- [31] R. Hlubina and T.M. Rice, Phys. Rev. B **51**, 9253 (1995).
- [32] A. Chubukov, Europhys. Lett. **44**, 655 (1997).
- [33] J. Schmalian *et al.*, Phys. Rev. Lett. **80**, 3839 (1998).
- [34] L.B. Ioffe and A.J. Millis, Phys. Rev. B **58**, 11631 (1998).
- [35] G. Blumberg *et al.*, preprint
- [36] The different background for the $9 \text{ K}/8 \text{ T}$ spectrum is due to RL polarization ($B_{2g} + B_{1g}$) used for scattering in magnetic field.
- [37] B. S. Shastry, and B. I. Shraiman, Phys. Rev. Lett. **65**, 1068 (1990).
- [38] In analogy to the sum rules for optical conductivity $I_\mu^{\text{inf}} = \int_0^{\text{inf}} \chi''_\mu/\omega d\omega$ is expected to be a temperature independent constant.

[§] To whom correspondence should be addressed. E-mail: girsh@bell-labs.com

[†] Permanent address: Institute of Solid State and Materials Research Dresden, P.O. Box 270016, D-01171 Dresden, Germany.

[¶] Permanent address: Centre de recherche sur les propriétés électroniques de matériaux avancés and Département de Physique, Université de Sherbrooke, Sherbrooke, Québec, CANADA, J1K 2R1.

- [1] T. Timusk and B. Statt, Rep. Prog. Phys. **62**, 61 (1999).
- [2] C.C. Tsuei and J.R. Kirtley, Phys. Rev. Lett. **85**, 182 (2000).
- [3] R. Prozorov *et al.*, Phys. Rev. Lett. **85**, 3700 (2000); J.D. Kokales *et al.*, Phys. Rev. Lett. **85**, 3696 (2000).
- [4] T. Sato *et al.*, Science **291**, 1517 (2001).
- [5] N.P. Armitage *et al.*, Phys. Rev. Lett. **86**, 1126 (2001).
- [6] G. Blumberg *et al.*, Phys. Rev. Lett. **88**, 107002 (2002).
- [7] A. Biswas *et al.*, Phys. Rev. Lett. **88**, 207004 (2002).
- [8] J.A. Skinta *et al.*, Phys. Rev. Lett. **88**, 207005 (2002).
- [9] C.C. Homes *et al.*, Phys. Rev. B **56**, 5525 (1997).